JACS
JOURNAL OF THE AMERICAN CHEMICAL SOCIETY
Article
pubs.acs.org/JACS

The Effect of Solvent Additives on Morphology and Excited-State Dynamics in PCPDTBT:PCBM Photovoltaic Blends

Fabian Etzold,[†] Ian A. Howard,[†] Nina Forler,[§] Don M. Cho,[‡] Michael Meister,[†] Hannah Mangold,[†] Jie Shu,[§] Michael Ryan Hansen,[§] Klaus Müllen,[‡] and Frédéric Laquai*[,†]

[†]Max Planck Research Group for Organic Optoelectronics, [§]Polymer Spectroscopy Group, and [‡]Synthetic Chemistry Group, Max Planck Institute for Polymer Research, Ackermannweg 10, 55128 Mainz, Germany

Supporting Information

ABSTRACT: The dependence of the thin film morphology and excited-state dynamics for the low-bandgap donor−acceptor copolymer poly[2,6-(4,4-bis-(2-ethylhexyl)-4*H*-cyclopenta[2,1-b;3,4-b′]-dithiophene)-*alt*-4,7-(2,1,3-benzothiadiazole)] (PCPDTBT) in pristine films and in blends (1:2) with [6,6]-phenyl-C_{61}-butyric acid methyl ester (PCBM) on the use of the solvent additive 1,8-octanedithiol (ODT) is studied by solid-state nuclear magnetic resonance (NMR) spectroscopy and broadband visible and near-infrared pump−probe transient absorption spectroscopy (TAS) covering a spectral range from 500−2000 nm. The latter allows monitoring of the dynamics of excitons, bound interfacial charge-transfer (CT) states, and free charge carriers over a time range from femto- to microseconds. The broadband pump−probe experiments reveal that excitons are not only generated in the polymer but also in PCBM-rich domains. Depending on the morphology controlled by the use of solvent additives, polymer excitons undergo mainly ultrafast dissociation (<100 fs) in blends prepared without ODT or diffusion-limited dissociation in samples prepared with ODT. Excitons generated in PCBM diffuse slowly to the interface in both samples and undergo dissociation on a time scale of several tens of picoseconds up to hundreds of picoseconds. In both samples a significant fraction of the excitons creates strongly bound interfacial CT states, which exhibit subnanosecond geminate recombination. The total internal quantum efficiency loss due to geminate recombination is estimated to be 50% in samples prepared without ODT and is found to be reduced to 30% with ODT, indicating that more free charges are generated in samples prepared with solvent additives. In samples prepared with ODT, the free charges exhibit clear intensity-dependent recombination dynamics, which can be modeled by Langevin-type recombination with a bimolecular recombination coefficient of 6.3×10^{-11} cm^3 s^{-1}. In samples prepared without ODT, an additional nanosecond recombination of polaron pairs is observed in conjunction with an increased intensity-independent trap-assisted nongeminate recombination of charges. Furthermore, a comparison of the triplet-induced absorption spectra of PCPDTBT with the charge-induced absorption in PCPDTBT:PCBM blends reveals that triplets have a very similar excited-state absorption spectrum compared to the free charge carriers, however, in contrast have a distinct intensity-independent lifetime. Overall, our results suggest that whether free charges or strongly bound CT states are created upon dissociation of excitons at the PCPDTBT:PCBM interface is determined instantaneously upon exciton dissociation and that once formed strongly bound CT states rapidly recombine and thus are unlikely to dissociate into free charges. The observation of a significantly larger bimolecular recombination coefficient than previously determined for poly(3-hexylthiophen-2,5-diyl):PCBM (P3HT:PCBM) and PCDTBT:PCBM samples indicates that nongeminate recombination of free charges considerably competes with charge extraction in PCPDTBT:PCBM photovoltaic devices.

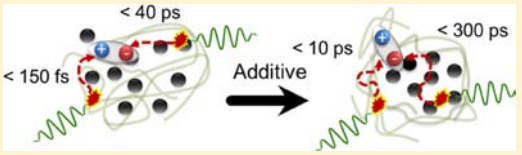

1. INTRODUCTION

Bulk heterojunction (BHJ) organic solar cells based on thin films of interpenetrating polymer:fullerene networks are an emerging technology that has the potential to provide a low-cost alternative to conventional silicon-based photovoltaic devices. Organic materials can easily be solution processed enabling large-area production of solar cells, for instance by roll-to-roll printing techniques.[1,2] Their efficiency, however, is still unsatisfactory for mass production leaving space for further improvements, if the efficiency-limiting processes can be understood and reliable structure−property relations can be developed.

In BHJ photovoltaic devices absorption of photons by one of the blend components leads to the formation of excitons, which undergo dissociation at the polymer:fullerene interface. The products of exciton dissociation are unbound (free) charge carriers and bound interfacial polaron pairs. In this context delocalization of the intermediate "hot" polaron pairs created during the exciton dissociation process at the interface has recently been shown to help overcome the exciton binding energy.[3] While the free charges can successively be extracted as photocurrent or undergo recombination according to a nongeminate (often also termed bimolecular) recombination pathway, the intermediate polaron pairs either can relax into strongly bound charge-transfer (CT) states that recombine to

Received: April 5, 2012
Published: May 21, 2012

   dx.doi.org/10.1021/ja303154g | *J. Am. Chem. Soc.* 2012, 134, 10569−10583

the ground state by a monomolecular (geminate) recombination process or could potentially split by a field- or temperature-assisted process (often described by the Onsager−Braun model), yielding free charges that can additionally contribute to the total photocurrent. However, it is difficult, if not impossible, to judge from the shape of the device $J-V$ curve, whether nongeminate recombination in competition with charge extraction or a field-assisted charge liberation from polaron pairs or a combination of both governs the bias-dependence of the photocurrent and thus determines the device fill factor. We and others have recently shown for the reference system poly(3-hexylthiophen-2,5-diyl):[6,6]-phenyl-C_{61}-butyric acid methyl ester (P3HT:PCBM) that nongeminate recombination in competition with charge extraction determines the bias dependence of the photocurrent in these devices and that free charge generation is neither a temperature- nor a field-activated process in optimized devices.[4−6] However, it appears that P3HT:PCBM is rather an exception than a prototypic system due to the high crystallinity of the P3HT network facilitating free charge generation and fast extraction, while simultaneously suppressing nongeminate recombination.[6] In order to develop a broader picture, it is thus important to better understand these processes in other systems, which are less ordered than the exceptional and well-studied case of P3HT:PCBM. In particular low-bandgap alternating donor−acceptor (DA) copolymers have emerged as promising electron-donor materials and have already proven their potential in highly efficient bulk heterojunction organic solar cells in combination with fullerene derivatives as electron acceptors.[7−11] Their absorption extends further into the red to near-infrared (NIR) spectral region of the solar spectrum, and thus low-energy photons are more efficiently harvested than, for instance, in P3HT:PCBM, for which typically only moderate efficiencies of around 3−4% are obtained, and the maximum efficiency is limited to 4.4% due to the limited overlap with the solar illumination.[12] In the OPV community the low-bandgap polymer poly[2,6-(4,4-bis-(2-ethylhexyl)-4H-cyclopenta[2,1-b;3,4-b′]-dithiophene)-alt-4,7-(2,1,3-benzothiadiazole)] (PCPDTBT) has attracted particular interest, since its absorption spectrum extends beyond 800 nm, and efficiencies as high as 5.5% have been demonstrated under optimized conditions.[7,13,14] Nonetheless, PCPDTBT-based devices often suffer from a low fill factor and in general have a lower internal quantum efficiency in comparison to P3HT:PCBM devices, i.e., the efficiency gain due to enhanced photon harvesting in the red part of the solar illumination is in part offset by enhanced loss processes. Introducing solvent additives to control the blend intermixing and morphology during the spin-coating process has been shown to significantly increase the device performance, which makes PCPDTBT an appealing study subject, since the efficiency increase should be reflected in a significant change of the photophysical properties.[7] The impact of solvent additives on the morphology has already been intensively investigated by structural probes, such as GISAXS, etc.[15,16] From a morphological viewpoint the superior device efficiency obtained from blends processed with additives has been attributed to enhanced demixing. This reduces the interfaces for recombination of charges and leads to an increased structural order within the polymer-rich domains, facilitating fast charge transport and extraction. However, a conclusive picture of the entire cascade of the photophysical processes leading to photocurrent generation and the changes introduced by the film processing parameters, such as additives, is still lacking.

Blom and co-workers have recently assigned the increased efficiency of PCPDTBT:PCBM blends processed with additives to reduced geminate recombination losses by fitting the experimentally obtained $J-V$ curves of devices using a drift-diffusion model for free charges and an additional Onsager-Braun type CT-state dissociation mechanism.[17] From their model they estimated the lifetime of interfacial CT states to be from 500 ns to 3 μs. Recent work by us and others has shown that the inverse rate of CT-state recombination is rather in the range of nanoseconds, and therefore the CT-state recombination rates extracted from modeling $J-V$ curves should rather be considered a fitting parameter than a rate related to a photophysical process. Very recently, McNeill and co-workers demonstrated that charge-carrier trapping and, thus, the dwell time of free charge carriers are reduced in devices processed with additives by measuring the transient photovoltage characteristics of PCPDTBT:PCBM cells, which indicates that the efficiency of PCPDTBT:PCBM cells prepared without additives is hampered by trap-assisted nongeminate recombination in competition with charge extraction.[18] Cho et al. measured the charge-carrier mobility in bipolar field-effect transistors (BIFETs) and found a higher mobility in blends processed with additives.[19] In contrast, time-of-flight studies, which probe the bulk mobility and thus deliver a more meaningful estimate of the mobility in photovoltaic devices, did not show a significant increase of the bulk mobility upon using additives.[20] Neher and co-workers have very recently reported time-delayed collection field experiments on PCPDTBT:PCBM blends.[21] They demonstrated that the yield of free charges increases upon applying a prebias during excitation indicative of a field-dependent charge-generation process, which was found to be more pronounced in samples prepared without 1,8-octanedithiol (ODT). Furthermore, they observed a negative field dependence of the hole mobility, which was assigned to spatial disorder, and a large bimolecular recombination coefficient on the order of 10^{-11} cm^3 s^{-1}, indicating fast nongeminate recombination of free charges. The observation of a field-dependent charge generation is in stark contrast to earlier results reported by Durrant and co-workers. They used bias-dependent transient absorption spectroscopy to monitor the amplitude and dynamics of the charge-induced absorption from 100 ns onward and found both the amplitude and dynamics to be independent of an external electric field.[22] In samples prepared with an additive, the amplitude of the charge-induced absorption was found to be increased by a factor of 1.5, pointing toward a more efficient generation of free charges in samples prepared with additives. However, the pump fluences used were typically higher than 8 $\mu J/cm^2$, at which nongeminate recombination of free charges within the first 100 ns can be expected due to their high concentration. In an earlier study Durrant and co-workers probed the delayed recombination of free charges by means of single wavelength TA spectroscopy and came to the conclusion that the presence of solvent additives changes the ionization potential (IP) of the polymer and thereby also the free energy of the charge transfer process, resulting in an increased yield of free polarons upon processing with additives.[23] In general, optical probes, such as time-resolved spectroscopy and in particular pump−probe spectroscopy, are very powerful tools to study the dynamics of charge generation and recombination and to develop a general picture of the photophysical processes, if the entire relevant

spectral and dynamic range can be investigated. For example, Hwang et al. have used (ultrafast) transient absorption spectroscopy to elucidate the early time (up to 1500 ps) charge generation and recombination dynamics in PCPDTBT:PCBM. They reported ultrafast (<200 fs) electron transfer at the polymer:fullerene interface resulting in the formation of mobile carriers (free polarons) and interfacial CT states, the latter either recombining to the ground state (<600 ps) or dissociating into free charges in less than 20 ps. In a subsequent study by Heeger and co-workers the effect of solvent additives and blend composition was investigated, and the authors concluded that films processed with additives and those containing larger PCBM fractions showed enhanced splitting of the interfacial CT states.[20,24] A severe drawback of these studies is the very high fluences (up to 200 $\mu J/cm^2$) used in their experiments, necessary to achieve a reasonable signal-to-noise ratio. Furthermore, Grancini et al. have recently investigated the effect of the fraction of PCBM and of the solvent additive on the charge generation and recombination dynamics and concluded that charge generation is possible via direct hot exciton dissociation and an Onsager-like dissociation process. They covered the time range up to 400 ps only, so that a clear picture of the long time recombination dynamics is still missing.[25] Jarzab et al. have recently determined the (fluorescence) lifetime of the emissive interfacial CT states (referred to as CT excitons) to be 480 ps by NIR streak camera measurements in samples prepared without additives.[26,27] They concluded that the emissive CT states observed by photoluminescence spectroscopy are strongly bound and cannot be split by a field- or temperature-activated process into free charges and thus rather recombine to the ground state. However, their bias-dependent photoluminescence spectra showed a reduction of the amplitude of the CT-emission indicating a bias-induced variation of the initial population of the CT states not resolved by the time resolution of their experiment. Very recent work by Deschler et al. showed that the initial fraction of free charges created directly after photoexcitation can be increased in PCPDTBT:PCBM films by deliberate doping, implying that the fate of the primary photoexcitation, i.e., whether free charges or CT states are formed upon exciton dissociation, is determined on the ultrafast time scale.[28] The fluorescence lifetime of the CT excitons was determined to be 300 ps in line with the results by Jarzab et al. Janssen and co-workers have observed that the interfacial CT state can also undergo intersystem crossing to populate the polymer's triplet state and that the morphology obtained by processing in the presence of solvent additives can suppress this additional loss channel.[29]

In the present work we used solid-state NMR techniques to investigate the morphology of thin films of PCPDTBT:PCBM processed with and without the solvent additive ODT and broadband visible to NIR (vis-NIR) pump−probe spectroscopy to optically probe the charge generation and recombination dynamics. In contrast to earlier ultrafast pump−probe and microsecond transient absorption studies, we also report the very important time range between 2 and 100 ns and thus are able to monitor the full recombination dynamics and accurately determine the ratio between monomolecular and non-monomolecular recombination. Additionally, we present not only pump−probe spectra in the visible wavelength range from 500 to 1000 nm but also in the NIR (1000−2000 nm) spectral region, which we acquired with our newly developed NIR broadband probe and detection scheme. The unique combination of an extended temporal and spectral pump−probe range allowed us: (i) to differentiate between the temporal evolution of excitons, free charges, and CT states due to their individual absorption profiles in the NIR; (ii) to determine the lifetime of strongly bound interfacial CT states as well as the nongeminate recombination coefficient and recombination order of free charges; (iii) to study the effect of solvent additives on the above-mentioned processes and (iv) to elucidate the role triplet states play in the photophysics of PCPDTBT:PCBM blends. We relate our findings to the significant change of the photovoltaic efficiency observed upon processing of the blend with solvent additives.

2. RESULTS

In this section we first present a morphological study on PCPDTBT:PCBM blends prepared with and without ODT as cosolvent performed by solid-state NMR spectroscopy. Prior to presenting the early time (ps−ns) exciton and charge generation dynamics in PCPDTBT:PCBM blends as well as the delayed (ns−μs) charge recombination and triplet state dynamics and the effect of the cosolvent/additive on the dynamics, we will also briefly report the exciton dynamics of pristine PCPDTBT polymer films measured by vis-NIR pump−probe spectroscopy as these will be relevant for the interpretation of the pump−probe spectra of the blends. We further note that all pump−probe transient absorption experiments presented in the following paragraphs have been repeated on separately prepared polymer films and blends at least two times and that the experimental results were found to be similar within the typical experimental error.

2.1. Influence of ODT on Morphology Studied by Solid-State NMR. Solid-state NMR can provide insights into the local order and packing arrangement of functional organic materials. Recent examples include discotic liquid crystals,[30,31] polymers,[32−34] pharmaceuticals,[35,36] and very recently also organic solar cell materials based on the BHJ principle, like P3HT:PCBM and PCPDTBT:PCBM blends.[37−39] In 1D ^{13}C magic-angle spinning (MAS) NMR spectra the isotropic ^{13}C chemical shift (δ_{iso}) position reflects the different chemical environments in the sample, and the ^{13}C linewidth can be used as a measure for the distribution of local geometries. This makes ^{13}C a sensitive probe toward structural order or disorder, which is further enchanced by its broad chemical shift dispersion (200 ppm) and thus high chemical shift resolution.[40] Moreover, the linewidths are not affected by homonuclear dipolar coupling due to the low natural abundance of ^{13}C (1.1%). Higher spectral resolution can be obtained by employing 2D heteronuclear correlation techniques, such as $^{13}C\{^1H\}$ Frequency-Switched Lee−Goldburg HETeronuclear CORrelation (FSLG-HETCOR).[41] Here, structural information about spatial proximities between ^1H and ^{13}C can be derived based on the distance-dependent strength of the dipole−dipole coupling between the nuclei. Furthermore, the resolution for ^1H is improved due to the application of FSLG homonuclear $^1H-^1H$ decoupling.[42]

Figure 1 shows 1D $^{13}C\{^1H\}$ CP/MAS NMR spectra of pure PCPDTBT and PCBM as well as blends of PCPDTBT:PCBM (1:2) processed with and without ODT. All materials except PCBM were drop-cast from *o*-dichlorobenzene (*o*-DCB).

The ^{13}C resonances of the pure PCPDTBT polymer in general exhibit narrower linewidths than those of both PCPDTBT:PCBM blends, indicating a lower degree of local ordering in the blend materials. In particular, the splitting of the

dx.doi.org/10.1021/ja303154g | J. Am. Chem. Soc. 2012, 134, 10569−10583

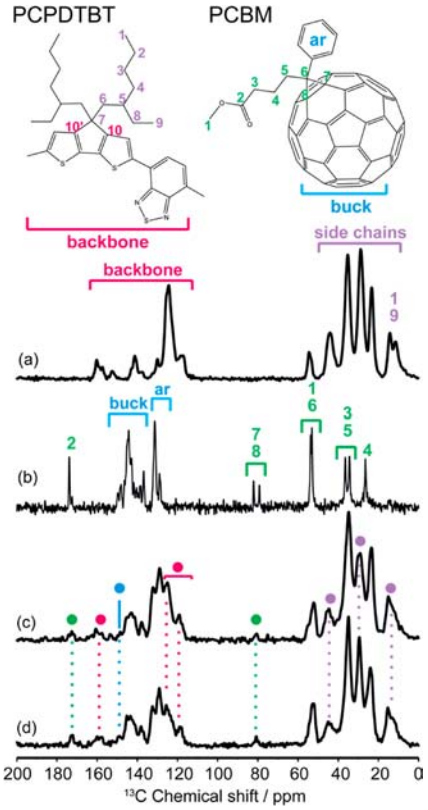

Figure 1. The top panel shows the chemical structures of PCPDTBT and PCBM. 1D $^{13}C\{^{1}H\}$ CP/MAS NMR spectra of (a) PCPDTBT, (b) PCBM, (c) PCPDTBT:PCBM (1:2), and (d) PCPDTBT:PCBM (1:2) processed with 2.4 vol % ODT. Apart from PCBM, which was used as a powder, all other materials were drop-cast from *o*-DCB. The assignment in (a–d) follows the color scheme given on the top. For the blends (c,d) the resonances that can be assigned unambiguously to PCPDTBT or PCBM are highlighted using the color scheme and marked with dashed lines.

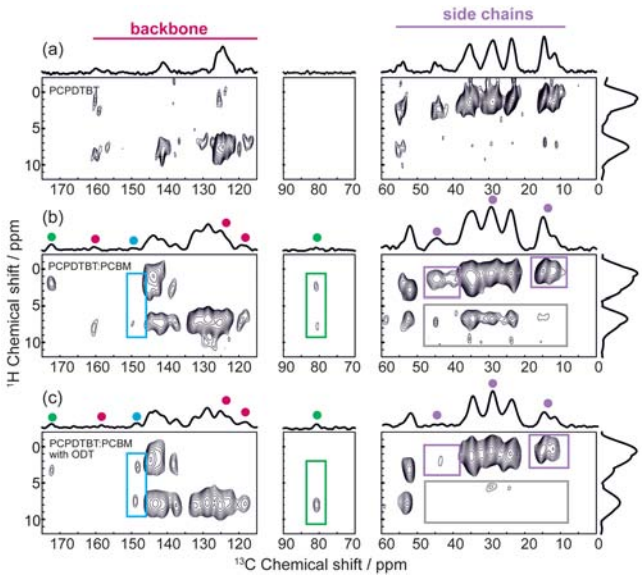

Figure 2. Selected regions of the 2D $^{13}C\{^{1}H\}$ FSLG-HETCOR NMR spectra for (a) PCPDTBT, (b) PCPDTBT:PCBM (1:2), and (c) PCPDTBT:PCBM (1:2) processed with 2.4 vol % ODT. All materials were drop-cast from *o*-DCB. The assignment is based on the color scheme given in Figure 1, and the main structural changes between (b) and (c) are marked with colored boxes. All spectra are plotted on the same intensity scale with contour lines from 10.1 to 90% of the maximum intensity.

signals from the methyl groups of PCPDTBT illustrates this behavior. For the pure PCPDTBT polymer, two well-resolved signals from the trans and gauche conformations (10–20 ppm) of the side-chain methyl groups arise, which in the case of the blends displays a broad overlap. This observation is in agreement with literature data where more amorphous environments in blends than in pure polymers have been reported.[43]

To gain a deeper insight into the local ordering and impact of ODT processing with respect to morphology, we have recorded 2D $^{13}C\{^{1}H\}$ FSLG-HETCOR NMR spectra of PCPDTBT and PCPDTBT:PCBM (1:2) blends as summarized in Figure 2.

In the 2D spectrum of the pure PCPDTBT polymer, all of the expected directly bound $^{1}H-^{13}C$ correlations are observed. However, no correlations between the hexyl–ethyl ($C_{6,2}$) side chains (0–60 ppm), attached at the bridging carbon of the fused dithiophene group, and the ^{1}H nuclei of the polymer backbone (>5 ppm) are observed. This suggests a well-defined packing arrangement of the PCPDTBT polymer with ordered regions for the $C_{6,2}$ side chains. In contrast, the PCPDTBT:PCBM (1:2) blend processed without ODT shows intense correlation peaks between aliphatic and aromatic moieties, see Figure 2b. The presence of these correlations suggests a homogeneous blend structure where the PCPDTBT polymer and PCBM acceptor of the BHJ are molecularly mixed, i.e., the alkyl side chains from PCPDTBT are in close proximity of the aromatic fragments of PCBM and vice versa. Interestingly, processing of PCPDTBT:PCBM (1:2) with ODT results in the disappearance of the correlation peaks between aliphatic and aromatic moieties as can be identified from Figure 2c. Furthermore, the processing with ODT leads to a signal reduction for the aliphatic groups related to the PCPDTBT polymer as marked in Figure 2c. This dramatic decrease in intensity can in principle result from the following evolutions of the PCPDTBT:PCBM blend morphology: First, the intermolecular interfaces can arrange in a more favorable manner, allowing the fullerene part of the PCBM to be in closer contact to the PCPDTBT polymer backbone. As a consequence, this leads to the elimination of alkyl–aromatic correlation peaks and to a more heterogeneous blend material. Second, the domain size in the blend material can grow due to the addition of ODT, which leads to a higher degree of demixing and a reduced number of intermolecular interfaces. Both of these changes in morphology do not exclude each other. AFM data (see Supporting Information, Figure S1) give evidence for increased domain sizes in the PCPDTBT:PCBM sample processed with ODT. In parallel, the 2D $^{13}C\{^{1}H\}$ FSLG-HETCOR spectrum of the blend processed with ODT (Figure 2c) exhibits correlation peaks that have narrower linewidths in both dimensions than the blend processed without ODT (Figure 2b). The latter observation points toward a higher degree of local ordering for both the PCPDTBT and PCBM domains upon addition of ODT. Thus, the addition of ODT results in a higher degree of demixing with increased domain sizes as well as in a higher degree of local order with better arranged intermolecular interfaces between donor and acceptor components of the BHJ. We note that similar conclusions about the increase in domain sizes upon processing with ODT (or other additives) have been

reported based on X-ray diffraction techniques for a number of different photovoltaic blends, including PCPDTBT:$PC_{70}BM$, PSBTBT:$PC_{60}BM$, and PTB-7:$PC_{70}BM$.[44−47]

2.2. Excited-State Dynamics in Pristine PCPDTBT. Due to the PCPDTBT polymer's long wavelength ground-state absorption extending up to 850 nm and the photoluminescence extending up to 950 nm, the excited-state photoinduced absorption (PA) features of the excitons are expected in the NIR probe range. Thus, we performed broadband NIR pump−probe spectroscopy covering the hitherto unobserved wavelength range from 1200−2000 nm in addition to pump−probe spectroscopy in the shorter wavelength region from 550−1050 nm, hereafter being referred to as visible wavelength region for reasons of simplicity.

Figure 3 displays examples of typical broadband visible and NIR pump−probe spectra from PCPDTBT thin films spin-cast

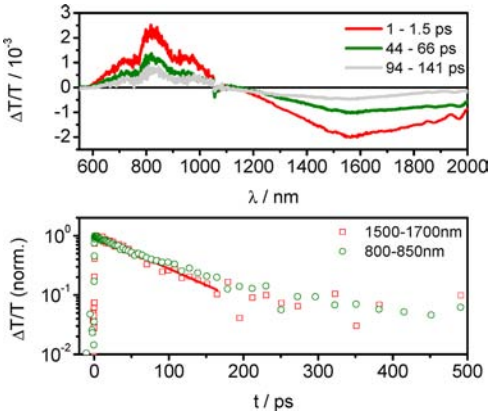

Figure 3. Early time transient absorption spectra of pristine PCPDTBT films spincast with ODT (top panel) excited with 5−6 $\mu J/cm^2$ at 550 nm. The bottom panel shows the dynamics of the stimulated emission and exciton-induced absorption on a semi-logarithmic scale including a single exponential fit to the NIR data with a lifetime of 78 ps.

with ODT monitored over a time range from one to several hundred ps using a low excitation fluence of 5−6 $\mu J/cm^2$ at 550 nm. The pump−probe spectrum of the polymer film shows distinct spectral features, namely a ground-state bleach (GSB) with an onset at 600 nm extending to 850 nm, where typically the ground-state absorption of the polymer is observed in steady-state absorption measurements, and a region of stimulated emission (SE) extending up to 1000 nm, which overlaps with the GSB in the shorter wavelength region. The wavelength region in which SE can be observed corresponds to the spectral region of fluorescence as both originate from the first excited singlet state. The dynamics of the SE signal, which tracks the population of singlet excitons, decays monoexponentially with a lifetime of 95 ps. The observed exciton lifetime is rather short, which must be a consequence of strong nonradiative deactivation processes competing with the emissive (fluorescent) decay of the exciton. This is in line with the low quantum yield of 6% recently reported for pristine PCPDTBT samples by Jarzab et al.[26] We note that the dynamics obtained by our pump−probe experiments are unaffected by higher order processes, such as exciton−exciton annihilation, since the pump fluence was kept well below the onset of these processes, which can be observed at higher fluences (see Supporting Information, Figure S2) and are typically indicated by accelerated exciton decay dynamics. The exciton lifetime we obtained from our pump−probe experiments is in excellent agreement with those recently reported by Jarzab et al., who determined the fluorescence lifetimes of PCPDTBT films by the streak camera technique.[26,27]

In the NIR spectral region of our pump−probe experiments we observe a photoinduced absorption covering the entire NIR wavelength range from 1200−2000 nm, which peaks at 1580 nm. In accordance with the visible pump−probe experiments, which showed stimulated emission indicating the presence of excited singlet states, we assign the PA to the presence of singlet excitons immediately generated after photoexcitation. The PA decay fits well to a single exponential with a lifetime of 78 ps, which is slightly shorter than observed for the visible pump−probe measurements, but within the experimental error of the experiment. We have also performed long-delay (ns−μs) pump−probe experiments on pristine PCPDTBT films and could observe a weak photoinduced absorption signal at 1300 nm with an approximate lifetime of 1 μs indicative of some triplet formation in the pristine polymer (see Supporting Information, Figure S3). In addition, low-temperature (80 K) steady-state photoinduced absorption measurements (PIA) on pristine PCPDTBT thin films also showed a double-peaked spectrum in the NIR typical of charge carriers in conjugated polymers, indicating that a fraction of excitons can undergo dissociation to charges even in the absence of an electron acceptor (see Supporting Information, Figure S4).

2.3. Photovoltaic Performance. In this section we report on the impact of the cosolvent on the device performance. For the PCPDTBT polymer used in the present study we obtained average power conversion efficiencies (PCE) of 1% (J_{SC} = 4 mA/cm^2, FF = 38%, V_{OC} = 0.56 V) from blends with $PC_{60}BM$ spin-cast from chlorobenzene solutions without ODT. The PCE was doubled to 2.1% (J_{SC} = 7 mA/cm^2, FF = 45%, V_{OC} = 0.6 V), when ODT was used as an additive during the spin-casting process, mainly due to an increased short circuit current and a minor improvement of the device fill factor, which is in line with previous studies on PCPDTBT:PCBM blends.[14,27] The $J-V$ curves of the devices are shown in Figure 4 alongside the steady-state absorption spectra of the thin films. EQE spectra can be found in the Supporting Information (Figure S5). While the qualitative effect of ODT is well reproduced in

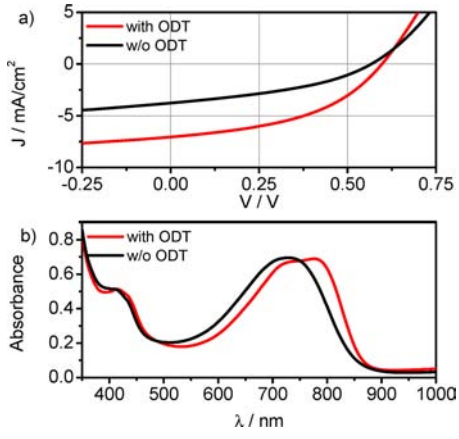

Figure 4. (a) $J-V$ curves of PCPDTBT:PCBM devices prepared with and without ODT. The PCE are 1% for the devices without ODT and 2% upon adding ODT. (b) Steady-state absorption of blend films prepared with and without ODT.

our present study, we found significantly lower average PCEs compared to the record efficiencies previously reported for this material system.[7] We would like to stress that several reasons can account for the lower average PCE compared to the record values, and we also note that the photovoltaic parameters are similar to those very recently reported by Scharber et al.[27] Among the most likely reasons: (i) a not fully optimized device structure; (ii) the use of $PC_{60}BM$ instead of $PC_{70}BM$, which inherently lowers the photon absorption of the blend; and (iii) the median molecular weight (M_n = 14.000 g/mol) of the polymer used for the present study. In particular the latter is known to have a pronounced effect on the PCE with higher molecular weights resulting in higher PCE values for reasons still not entirely understood. We note that we have used $PC_{60}BM$ for the present study to avoid a contribution of excited states on the fullerene to the pump–probe spectra of the blend, which can be neglected due to the comparably small excited-state cross sections of PCBM that would otherwise complicate the interpretation of the pump–probe spectra.[48] As has already been demonstrated by others, the ground-state absorption of the blend prepared with ODT is red-shifted compared to blends prepared without ODT and also exhibits a vibronic shoulder at the low-energy edge of the absorption spectrum (compare data in Figure 4b). This has previously been interpreted as increased order and enhanced component demixing in blends prepared with ODT and is well in line with the solid-state NMR results presented above. In comparison the blend film prepared without ODT shows a blue-shifted and less structured absorption spectrum indicative of a more amorphous film also implying smaller and less ordered polymer domains in line with our results obtained from solid-state NMR spectroscopy (see Section 2.1).

2.4. Early Time (ps–ns) Dynamics in PCPDTBT:PCBM Blends. In this section we present the early time (ps–ns) vis-NIR pump–probe spectra of PCPDTBT:PCBM (1:2) blends and the dynamics of charge formation and early time recombination studied by ultrafast transient absorption pump–probe spectroscopy.

2.4.1. Pump–Probe Spectra and Dynamics in the Visible. The early time (ps–ns) pump–probe spectra and dynamics of PCPDTBT:PCBM blends prepared without ODT can be found in Figure 5, while the spectra and dynamics for the films prepared with ODT are presented in Figure 6. Figures 5a and 6a display the pump–probe spectra of the respective sample, Figures 5b and 6b show the dynamics probed at the wavelength regions indicated, and Figures 5c and 6c show the intensity dependence of the dynamics monitored at the indicated spectral position. The early time visible pump–probe spectra of both samples exhibit two characteristic features, i.e., a positive signal in the shorter wavelength region from 600 to beyond 800 nm and a negative signal at longer wavelength extending further into the NIR beyond 1050 nm, which is typically the detection limit in visible pump–probe experiments, when silicon photodetectors are used. In line with the early time pump–probe spectra of the pristine film, the former can be assigned to the polymer's GSB. The latter is assigned to the onset of the charge-induced absorption.

The absence of any stimulated emission previously observed for wavelengths above 800 nm indicates rapid quenching and dissociation of the majority of the singlet excitons of the polymer at the PCPDTBT:PCBM interface. However, we will show later that some picosecond diffusion-limited dissociation of PCBM excitons occurs and that an additional diffusion-limited dissociation of polymer excitons can be observed in samples prepared with ODT. In both samples a small dynamic red-shift of the GSB over the entire nanosecond time scale is observed, indicating relaxation of the charges within the density of states. The red-shift is more pronounced in the sample prepared without ODT demonstrating that on the nanosecond time scale, charges relax into deeper tail states of the density of states, which is an indication of larger energetic disorder of the blend prepared without ODT. The sample prepared without ODT first exhibits a rise of the GSB followed by a decay of about 50% in the first 3 ns. In comparison, the blend prepared with ODT shows a decay of the bleach of only 30% after the signal rise, indicating a smaller fraction of geminate recombination and thus a larger fraction of free charge generation. To account for spectral relaxation of the bleach, the kinetics were extracted by tracking the maximum amplitude instead of using a single wavelength only. The reduced decay in the blend with ODT is in line with the results of Hwang et al., who deduced a reduction of the early time carrier loss (geminate recombination) in samples processed with ODT. However, they obtained a difference of 10% only, while here we observed a difference of 20%.[20] The dynamics of the GSB cannot be unambiguously assigned to a single photophysical process, since the recovery of the GSB represents the sum of the dynamics of all excited states present in the blend. In addition, the GSB can be superimposed by spectral relaxation phenomena and thermal effects, as has recently been suggested for P3HT:PCBM, and thus the absolute fractions of geminate recombination deduced from the ground-state recovery bear some uncertainty.[49]

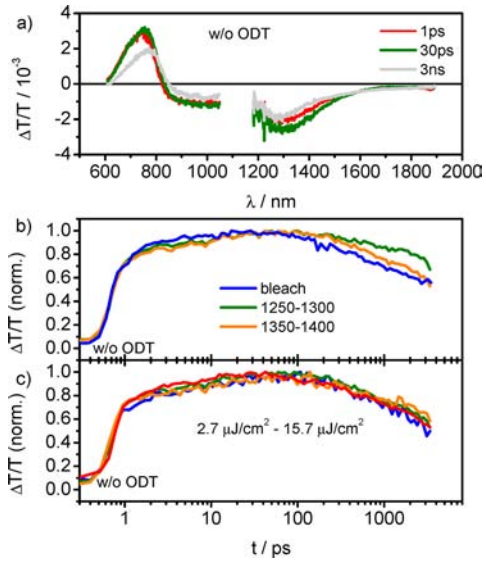

Figure 5. (a) Short delay (ps–ns) broadband transient absorption spectra of PCPDTBT:PCBM (1:2) blends prepared without ODT measured in the visible (600–1050 nm) and NIR (1100–1900 nm) spectral region at delay times of 1 ps (red), 30 ps (green), and 3 ns (gray). The pump fluence at 530 nm was 4.9 $\mu J/cm^2$ for the visible and 5.4 $\mu J/cm^2$ for the NIR measurements. (b) Short delay recombination dynamics of the photoinduced absorption probed at different wavelength regions in PCPDTBT:PCBM (1:2) blends prepared without ODT. (c) Intensity dependence of the early time dynamics tracked at 1350–1400 nm. Note that the dynamics are independent of pump fluence and the decay follows a single exponential with a mean lifetime of 1200 ps.

dx.doi.org/10.1021/ja303154g | J. Am. Chem. Soc. 2012, 134, 10569–10583

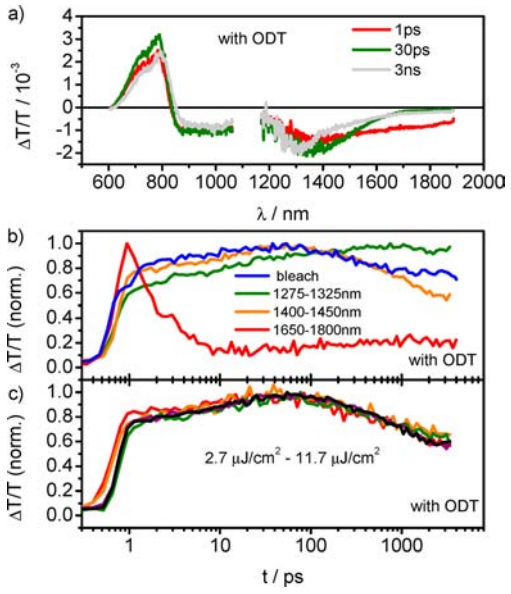

Figure 6. (a) Short delay (ps−ns) broadband transient absorption spectra of PCPDTBT:PCBM (1:2) blends prepared with ODT measured in the visible (600−1050 nm) and NIR (1100−1900 nm) spectral region at delay times of 1 ps (red), 30 ps (green), and 3 ns (gray). The pump fluence at 530 nm was 4.0 μJ/cm^2 for the visible and 3.9 μJ/cm^2 for the NIR measurements. (b) Early time dynamics of the exciton-induced absorption (1650−1800 nm) and the charge-induced absorption probed at different wavelength regions. Note the rapid decay of the signal in the region between 1650−1800 nm due to the diffusion-limited charge generation from polymer excitons. (c) Fluence dependence of the kinetics between 1400 and 1450 nm. The decay follows a single exponential with a mean lifetime of 700 ps.

As has already been mentioned above at longer wavelength, i.e., lower photon energy, the onset of the broad PA of charges can be observed in both blend films. The zero crossing between bleach and PA occurs at 825 nm for the blend prepared without ODT and at 835 nm for the blend prepared with ODT, respectively. Interestingly, the latter exhibits a more pronounced PA signal between 850−950 nm in contrast to the PA of the former. The appearance of a PA feature in this spectral region has previously been assigned to the presence of interfacial CT states, and its amplitude has qualitatively been correlated with the device performance by Hwang et al.[20,24] Here we observe a more pronounced PA from the blend prepared with ODT, which is inconsistent with the results of Hwang et al., who found that the PA in this spectral region vanishes if the sample is prepared with ODT and interpreted this to be due to more efficient splitting of CT states. In the present case we hypothesize that this feature may rather be related to the degree of order of the polymer-rich regions and the amount of demixing of the blend. We note that in the present study we have investigated PCPDTBT:PCBM blends with a ratio of 1:2. In fact, for this ratio Hwang et al. observed similar spectral features in line with our observations, which were reduced at higher PCBM concentrations of 1:3.6, suggesting a lower degree of order for the polymer domains at higher PCBM fractions.

On the basis of the above results we note that a clear assignment of the charge-induced PA signal seen in the visible pump−probe spectra appears difficult as only the tail can be observed up to 1050 nm, which, as we will show below, can reveal neither the conversion from excitons to interfacial CT states and free charges nor the individual recombination dynamics of free charges, trapped charges, and CT states. Quasi-steady-state photoinduced absorption (PIA) spectroscopy has previously demonstrated that the charge-induced absorption in PCPDTBT:PCBM peaks at around 1300 nm and extends even further into the NIR (see Supporting Information, Figure S6).[29] However, PIA probes a lifetime and concentration averaged sum of the ensemble of all excited states under quasi-equilibrium conditions, and for this reason only provides very limited or no information about the spectral profiles of individual states, especially if they are very short-lived as can be expected for CT states or singlet excitons. In addition a quantitative assessment of PIA data is difficult, as the cross sections of the species are typically not known. Hence, we have monitored the spectral profiles and dynamics of the entire charge-induced absorption in the NIR spectral region using a novel broadband NIR pump−probe setup and NIR detection scheme described in detail in the experimental part.

2.4.2. Pump−Probe Spectra and Dynamics in the NIR Region. Typical ps−ns NIR pump−probe spectra obtained for blends prepared without and with ODT are also presented in Figures 5 and 6, respectively, along with the visible pump−probe spectra discussed in the previous paragraph. In the following we will first concentrate on the results obtained for the sample prepared without ODT and then compare these results to those obtained for the sample prepared with ODT. The charge-induced PA of the sample prepared without ODT is rather broad spanning the entire NIR wavelength range from 1150−1900 nm. Figure 5b presents the dynamics of the PA signal probed at different wavelength regions. All dynamics exhibit an ultrafast rise due to the convolution of the pump and probe pulse lengths limiting the temporal resolution of our experiment to 100 fs. An additional slower but significant rise of the charge-induced PA signal within the first 50 ps is observed for the dynamics monitored between 1400−1450 nm. As can be seen from the spectra in Figure 5a, the amplitude of the bleach follows a similar rise over the same period of time, indicating that during the first 50 ps we observe a delayed generation of charges and CT states. Such a rise of the charge-induced absorption has previously been assigned in other polymer:fullerene systems to either a delayed transition from singlet excitons to charges or a liberation process of free charges from a precursor state, for instance, an intermediate polaron pair, that can either split into free charges or relax into strongly bound interfacial CT states.[50] We emphasize that in the latter case of a transition from intermediate polaron pairs to free charge carriers or CT states, a constant amplitude of the bleach during the conversion process is expected. This was not observed in our measurements. Furthermore, we rule out exciton diffusion in the polymer on the time scale of several tens of picoseconds as we observe neither stimulated emission nor the typical exciton-induced absorption, which, as we will show later, can be detected in samples prepared with ODT at wavelengths longer than 1600 nm in the first 10 ps. Hence, the most likely explanation is that we observe a prolonged diffusion of excitons in PCBM-rich domains, which are subsequently quenched at the interface, causing a signal rise of the polymer bleach due to the hole transfer to the polymer. To further support this interpretation, we repeated the measurements using a pump wavelength of 700 nm, where the fraction of polymer absorption was significantly larger compared to the absorption of PCBM, and thereby, a reduced amount of PCBM excitons is generated. Interestingly, upon excitation at 700 nm

the amplitude of the signal rise during the first 50 ps was reduced to less than 10% in contrast to the 20% amplitude increase observed after excitation at 532 nm. The dynamics after excitation at 700 nm can be found in the Supporting Information (Figures S7 and S8). Unfortunately, it is not possible to decompose the NIR spectrum into the individual photoinduced absorption spectra of free charges and bound polaron-pairs, since their absorption spectra are virtually similar, and thus the spectra and dynamics that we probe between 1250−1400 nm consist of contributions from both bound polaron-pairs and free charge carriers. We also note that Janssen et al. have recently reported that in samples prepared without ODT, the CT state can undergo intersystem crossing to a triplet state.[29] The latter could have a larger cross-section and could also cause a signal rise in the observed spectral region if CT states are converted into triplets, which is addressed later. After the initial clear signal rise caused by diffusion-limited exciton dissociation in the PCBM domains, we observe a large decay of the entire charge-induced PA band occurring within the time scale of the early time pump−probe experiment in line with the significant nanosecond decay of the GSB. The dynamics on this time scale can be fitted with a single exponential yielding a lifetime of 1200 ps, depending slightly on the signal offset used for fitting. Most importantly we found that neither the dynamics of the rise nor the early time decay between 1350−1400 nm are fluence dependent, i.e., they do not depend on the initial concentration of excited states as can be clearly seen in Figure 5c. In case of the signal rise, this indicates that prior to exciton dissociation we do not observe exciton annihilation at the pump fluences used, and in case of the decay, it proves that we observed a geminate recombination process of strongly bound and thus localized interfacial CT states that undergo nanosecond recombination to the ground state and cannot dissociate into free charges. Interestingly, the inverse recombination rate we obtained from the decay is in excellent agreement with the decay time recently reported for the CT state emission from PCPDTBT:PCBM blends by Jarzab et al., supporting our interpretation that here we indeed observe the recombination dynamics of relaxed (and thus luminescent) CT states.[26,27]

We now examine the NIR features observed for the blend prepared with ODT. Figure 6 shows the NIR pump−probe spectra and dynamics in different wavelength regions and the intensity dependence of the NIR PA signal dynamics. Before starting a detailed description, it is worth emphasizing that the NIR pump−probe spectra of the sample prepared with ODT contain significantly more spectral features than the NIR spectra obtained for the sample prepared without ODT. These features visible in the NIR contain significantly more information than those in the visible pump−probe spectra, allowing us to clearly recognize the dynamics of the individual species present in the blends. The following features can be identified in the blend prepared with ODT: (i) a rather short-lived PA between 1600 to 1900 nm that extends further into the IR region decaying within a few ps; (ii) a broad PA between 1400 and 1500 nm vanishing within several hundred ps; and (iii) a comparably narrow PA with a maximum at 1300 nm that continuously rises over the first 300 ps and then stays virtually constant on the investigated time scale. By comparing the NIR spectra of the blend to those of the pristine polymer shown in Figure 3, we conclude that the spectral region between 1600 to 1900 nm is dominated by polymer exciton-induced absorption and that the very short-lived feature seen in this spectral region is caused by polymer singlet excitons that must diffuse to an interface prior to their dissociation. The early time decay transients monitored from 1650−1800 nm, shown in Figure 6b, further reveal that the polymer excitons are entirely quenched after 10 ps in the blend with ODT. This is in contrast to the results obtained for the blend prepared without ODT where the polymer exciton-to-charge conversion happens on a time scale faster than the time resolution of our setup. The straightforward explanation for the difference is a change of the morphology toward enhanced demixing and polymer-enriched domains in the film prepared with ODT as a cosolvent, which is in line with our morphology studies by solid-state NMR techniques presented above.

The second feature that can be identified in the blend prepared with ODT is most prominent between 1400−1500 nm. Here, we again observed a rise of the signal similar to the sample prepared without ODT described above, followed by a decay extending to several nanoseconds. We extracted the dynamics for this spectral region and found the decay of the signal to follow a single exponential with a lifetime of about 700 ps (see Figure 6b). The lifetime was also found to be independent of the excitation intensity, and thus this decay can be assigned to CT states undergoing a monomolecular geminate recombination process. Interestingly, the lifetime of the geminate recombination is shorter compared to the recombination time observed for the CT excitons in the sample prepared without ODT. The decay observed in this spectral region is accompanied by a significant signal loss of the GSB observed in the visible pump−probe experiments, further supporting that these states return to the ground state on a subnanosecond time scale. The third feature, which is most prominent between 1275 and 1325 nm, remains after the decay of the signal between 1400 and 1500 nm is completed. In this spectral region we observe a clear signal rise up to several hundred picoseconds, after which the signal remains virtually constant in contrast to the measurements presented for the sample prepared without ODT. The observation of a first increasing and afterward constant signal at 1300 nm can be explained by diffusion-limited exciton dissociation in polymer and PCBM-rich domains. While the former appears to be completed after 10 ps, the latter process continues up to several hundred picoseconds in samples prepared with ODT, suggesting larger PCBM-rich domains in samples prepared with ODT. The significantly narrower charge-induced absorption peak that remains after 3.5 ns in the sample prepared with ODT compared to the broad PA observed in the sample prepared without ODT (compare also long delay spectra) also implies that the free charge carriers are mostly present in more ordered polymer-rich regions, while in the blend prepared without ODT, the charges remain in disordered and amorphous regions, in agreement with the morphology changes induced by ODT.

2.5. Delayed (ns−μs) Pump−Probe Spectra and Dynamics. *2.5.1. Pump−Probe Spectra in the Visible and NIR.* Having presented the early time charge generation and CT-state recombination dynamics in PCPDTBT:PCBM blend films as a function of the processing additive, we will now turn to the charge recombination occurring on a time scale from 1 ns to tens of μs, in which we probe the dynamics of long-lived charge carriers that can potentially contribute to the device photocurrent. Figure 7 compares the visible and NIR pump−probe spectra between 1 ns and 1 μs of both blends, i.e., the blend prepared with and without ODT in Figure 7a,b,

dx.doi.org/10.1021/ja303154g | J. Am. Chem. Soc. 2012, 134, 10569−10583

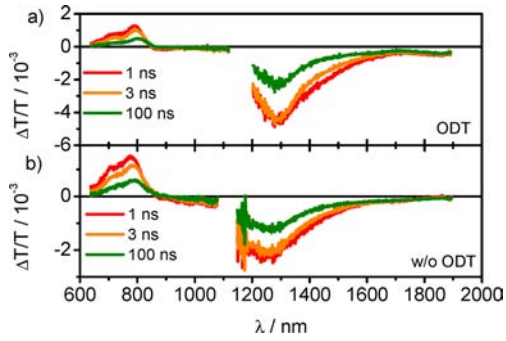

Figure 7. (a) Long delay (ns–μs) broadband transient absorption spectra of PCPDTBT:PCBM (1:2) blends prepared with ODT measured in the visible (600–1000 nm) and NIR (1100–1900 nm) spectral region at delay times of 1 ns (red), 3 ns (orange), and 100 ns (green). The samples were excited at 532 nm with a pump fluence of 8.7 μJ/cm^2 for the visible and 9.6 μJ/cm^2 for the NIR measurements. (b) Long delay (ns–μs) broadband transient absorption spectra of PCPDTBT:PCBM (1:2) blends prepared without ODT measured in the visible (600–1000 nm) and NIR (1100–1900 nm) spectral region at delay times of 1 ns (red), 3 ns (orange), and 100 ns (green). The samples were excited at 532 nm with a pump fluence of 6.1 μJ/cm^2 for the visible and 5.7 μJ/cm^2 for the NIR measurements.

respectively. As has already been evident from earlier experiments, the sample prepared with ODT exhibits stronger pronounced vibronic features of the GSB. From the shape of the GSB, it appears that those states surviving the first ns are mostly present in the more ordered regions of the polymer, while this is not the case for the sample prepared without ODT, which is in general less ordered. The dynamics of the GSB strongly depend on the spectral position probed, and it is therefore difficult to extract meaningful lifetimes and recombination dynamics as the recovery of the ground state mirrors the entire ensemble of excited states and their dynamics and is also subject to further spectral relaxation. The latter continues up to 100 ns in both samples, suggesting that charges slowly relax into tail states in the density of states. We note further that the charge PA in the visible spectral region is almost vanished for the sample prepared with ODT, while the onset can still be seen as a very weak signal in the sample prepared without ODT. The weak signal intensity of the charge-induced absorption in the visible spectral range complicates a meaningful extraction of the dynamics at times longer than several nanoseconds. However, the NIR spectral range still allows monitoring the charges, since the cross-section of charges in this spectral region is significantly larger than in the visible spectral region.

The samples prepared without ODT exhibit a peak of the charge-induced PA at 1240 nm, while the charge-induced absorption in the sample prepared with ODT peaks at 1285 nm. The first time slice measured for the sample prepared with ODT still shows a shoulder between 1400 and 1600 nm, which we have previously assigned to the presence of strongly bound interfacial CT states in the early time experiments. These CT decay dynamics are not resolved in the long delay experiment due to the limited time resolution (1 ns). Compared to the sample prepared without ODT, the peak is also narrower indicating that charges reside in more ordered domains in the blend prepared with ODT.

2.5.2. Spectra and Dynamics of Triplet States. A blue-shift of the NIR PIA band in samples prepared without ODT compared to samples prepared with ODT has very recently been reported by the Janssen group and was interpreted as evidence for enhanced triplet formation due to fast intersystem crossing from the CT state.[29] This process was found to be suppressed in samples prepared with ODT, which could in part explain the higher efficiency of these samples. However, triplet formation would require very fast intersystem crossing from the singlet CT state, which appears to be rather unlikely given the short subnanosecond CT recombination lifetime of strongly bound CT states observed in our early time experiments. On the other hand, some fraction of triplet formation cannot be entirely ruled out, as the position of the triplet-induced absorption is very similar to the absorption of charges, making them very difficult to distinguish from each other.[29] Therefore, to further elucidate the role of triplets, we studied thin films of PCPDTBT blended with a triplet sensitizer, namely platinum-octaethylporphyrin (PtOEP). PtOEP can be selectively excited into the Q-band at 532 nm, where the polymer absorption is weak. Upon excitation at 532 nm, the PtOEP singlet state is generated and rapidly converted into the triplet state. The triplet energy of PtOEP is around 1.9 eV and thereby significantly higher than the triplet of the polymer, allowing very efficient downhill Dexter-type triplet transfer from the sensitizer to the polymer. Some singlet energy transfer from the PtOEP to the polymer may also occur by Förster-type energy transfer, but due to the rapid ISC of PtOEP and short singlet state lifetime of PCPDTBT, the influence of singlet excitons on the PA spectrum can be neglected after 1 ns.

Figure 8 compares the NIR pump–probe spectra of the PCPDTBT:PtOEP blend with those obtained from a

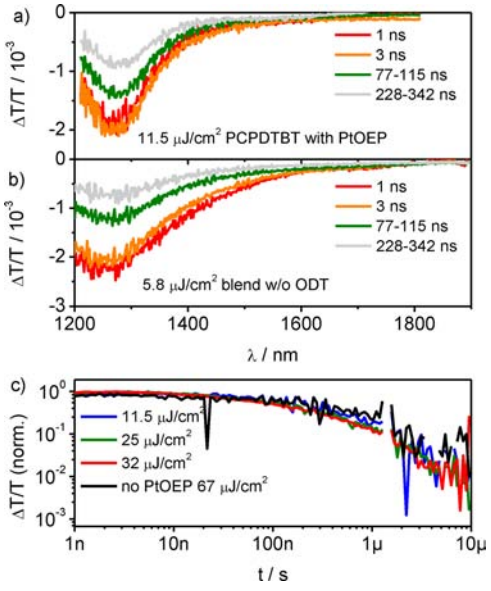

Figure 8. (a) NIR TA spectra of PCPDTBT blended with 40 wt % PtOEP and (b) NIR TA spectra of PCPDTBT:PCBM without ODT. (c) Fluence dependence of the triplet kinetics in the sample with PtOEP between 1250 and 1300 nm and for comparison the kinetics in the pristine polymer film (black line).

PCPDTBT:PCBM blend prepared without ODT and shows the intensity dependence of the triplet state decay dynamics. The peak position of the triplet-induced absorption is indeed very similar to the charge-induced absorption as reported by Janssen et al.[29] However, the triplet-induced absorption signal is much narrower than the charge-induced absorption seen in both blends. Furthermore, the decay dynamics we observed for

dx.doi.org/10.1021/ja303154g | J. Am. Chem. Soc. 2012, 134, 10569–10583

the triplet states are intensity-independent and very long-lived (1 μs) in contrast to the nongeminate charge recombination.

The unique long-lived, intensity-independent decay dynamics of the triplet excitons allows us to differentiate between triplet excitons and charges despite their similar spectral features. We will see that the absence of a 100 ns lifetime intensity-independent signal in the dynamics of the blends strongly suggests that no significant number of triplets is formed in the blends and that the differences in spectral features and kinetics in the blends can exclusively be explained in terms of differences in the charge populations.

2.5.3. Delayed (ns–μs) Recombination Dynamics of Charges. Figure 9 compares the dynamics of the charge-

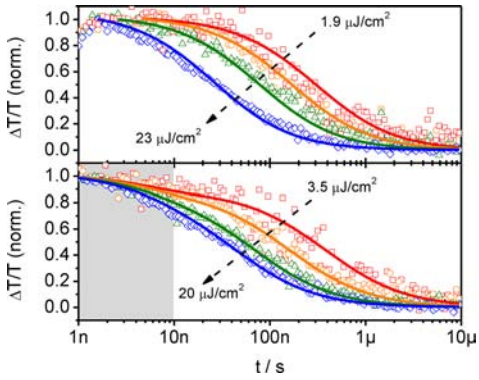

Figure 9. Intensity dependence of the long delay (ns–μs) decay dynamics of the charge-induced absorption in PCPDTBT:PCBM (1:2) blends prepared with ODT (top) and without ODT (bottom). The open symbols correspond to the experimental data, and the solid lines are fits obtained from a photophysical model as further described in the text. Note that in the bottom panel the additional intensity-independent decay phase has been highlighted by a light-gray box.

induced PA band for both PCPDTBT:PCBM blends monitored at the peak position. In the sample prepared without ODT, we observe an additional 10% signal loss during the first 10 ns even for the lowest excitation intensity. This is a significantly longer time scale than expected from the subnanosecond geminate recombination observed in the short-delay pump–probe experiments, which cannot be resolved here due to the poorer time resolution of our long-delay setup. The initial recombination exhibits a weak intensity dependence, and we therefore assign this process to recombination of loosely bound electron–hole pairs that cannot entirely escape their mutual coulomb attraction and thus have not managed to fully separate into free polarons. They undergo a slower nanosecond geminate recombination process, which is different from the fast geminate recombination of strongly bound interfacial CT states. After this initial recombination the dynamics clearly deviate from each other and become intensity dependent, indicating the recombination of separated charge carriers that undergo a nongeminate recombination process. The nongeminate recombination continues to about 10 μs, after which we could not obtain a meaningful residual signal anymore due to the limited signal-to-noise ratio. We have further analyzed the experimental data by fitting it to a previously introduced model that assumes a fraction of monomolecular polaron pair recombination and a separate fraction of nongeminate recombination of free charges without any interconversion between the two individual pools.[6] Using this model we could obtain an average decay time of the loosely bound polaron pairs in PCPDTBT:PCBM of 5 ns and a nongeminate recombination coefficient of 4×10^{-10} $(\mathrm{cm}^3)^{\lambda}/\mathrm{s}$ with a recombination order of $\lambda + 1 = 1.93$ in samples prepared without ODT as shown in Table 1. The order of recombination

Table 1. Fit Parameters Extracted Form Long Delay TA Measurements[a]

parameter	with ODT	without ODT
$\lambda + 1$	1.86 ± 0.01	1.93 ± 0.01
$\gamma/(\mathrm{cm}^3)^{\lambda}\ \mathrm{s}^{-1}$	$(1.0 \pm 0.4) \times 10^{-8}$	$(4 \pm 2) \times 10^{-10}$
f	1	0.89 ± 0.01
k_{LBP}/s^{-1}	absent	$(1.9 \pm 0.5) \times 10^{8}$

[a] $\lambda + 1$ describes the order of the decay, γ is the nongeminate recombination coefficient, f equals the fraction of nongeminate recombination, and k_{LBP} is the geminate recombination rate of loosely bound polaron pairs.

suggests a 3D Langevin-type of recombination with an effective (bimolecular) recombination rate of 3.2×10^{-11} cm^3/s at a charge-carrier density of 5×10^{15} $1/\mathrm{cm}^3$.

In comparison to the blend prepared without ODT the dynamics of the charge-induced absorption probed at 1300 nm are significantly different in the sample prepared with ODT. Here we observe a very pronounced intensity dependence of the dynamics from the earliest delay times onward. In fact, the intensity-independent component observed in the sample prepared without ODT is entirely absent. At the lowest pump fluence (1.9 $\mu\mathrm{J}/\mathrm{cm}^2$) that we probed, the charge-induced absorption is virtually constant within the first 10 ns, indicating that nongeminate recombination does not affect the dynamics on this time scale if the pump fluence is kept sufficiently low. It is also apparent from the dynamics in the first 10 ns that with increasing pump fluence, i.e., higher charge-carrier density, nongeminate recombination is present even at very early times below 10 ns. We note that the onset of nongeminate recombination occurs at pump fluences much lower than used in previous transient absorption studies.[20,24] At the highest pump fluence measured in our experiment, free charge carriers undergo nongeminate recombination from the earliest times (1 ns) onward. This implies very fast recombination, and thus a large nongeminate recombination coefficient as will be deduced below. In order to gain further information about the nongeminate recombination dynamics, we fitted the experimental data to the same model used for the sample prepared without ODT, this time assuming exclusively Langevin-type recombination for the sample prepared with ODT, since any nanosecond geminate component due to loosely bound polaron pairs appears to be entirely absent. The results of the fitting procedure are again depicted in Figure 9 as solid lines overlaying the experimental data (open dots). For the sample prepared with ODT, the dynamics can be described with a recombination order of $\lambda + 1 = 1.86$ and a nongeminate recombination coefficient of 1×10^{-8} $(\mathrm{cm}^3)^{\lambda}/\mathrm{s}$. From this an effective (bimolecular) Langevin recombination rate of 6.3×10^{-11} cm^3/s at a charge-carrier density of 5×10^{15} $1/\mathrm{cm}^3$ can be calculated. This is significantly larger compared to values that we have recently obtained by pump–probe spectroscopy on other polymer:fullerene blends, such as P3HT:PCBM and PCDTBT:PCBM,[6,51] and indicates that fast nongeminate recombination occurs even in PCPDTBT:PCBM blends prepared with ODT. The pronounced intensity dependence observed for the charge-induced absorption at 1300 nm, which

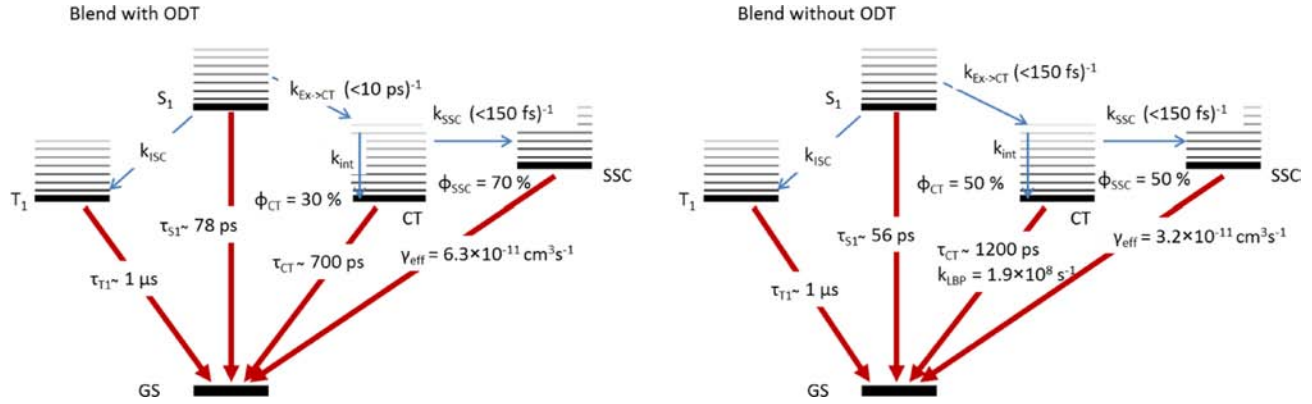

Figure 10. Scheme of the photophysical processes and their respective rates and lifetimes in PCPDTBT:PCBM blends processed with (left) and without (right) ODT. Upon excitation of the polymer, the excitons are quenched with a rate $k_{Ex\rightarrow CT}$, followed by the creation of spatially separated charge carriers (SSC) with the rate k_{SSC} or cooling of the CT state with the rate k_{int}. $\varphi_{SSC/CT}$ denotes the yield of the spatially separated charges and CT states, respectively. γ_{eff} is the effective bimolecular recombination coefficient of free charges, and τ_{CT} is the inverse geminate recombination rate of CT states to the ground state (GS). k_{ISC} is the intersystem crossing rate to the triplet level (T1), and $\tau_{T1/S1}$ is the lifetime of the singlet (S1) or triplet state in the pristine polymer, respectively. In the blend without ODT k_{LBP} describes the recombination rate of loosely bound polaron pairs.

is prominent even at early times, lets us conclude that around the PA peak position, we mainly probe the dynamics of the pool of free charge carriers. If we probe the dynamics at longer wavelength, for instance between 1450−1500 nm or even further in the NIR, the intensity dependence is much less pronounced, indicating that the charges that contribute to the PA in this wavelength region are much less mobile, i.e., present as trapped charges, and thus do not follow the same intensity dependent nongeminate Langevin-type recombination process. This effect is even more pronounced in case of the PCPDTBT:PCBM blend prepared without ODT. While we observed a pronounced intensity-dependent decay at a probe wavelength of 1260 nm (where the contribution of free charges is expected to be highest), the dynamics at longer wavelengths are virtually independent of the excitation intensity, indicating significant trapping and trap-assisted recombination of charges in samples prepared without ODT (see Supporting Information, Figure S10). Hence, it appears that ODT facilitates formation of mobile charge carriers, which recombine according to an intensity-dependent nongeminate recombination process and thus can escape trap-assisted recombination. In agreement with previous studies we also observe that if we take the early time (1 ns) amplitude at the peak position of the charge-induced absorption as a measure of the efficiency of free charge generation, a 1.5 times higher signal amplitude for samples prepared with ODT is observed compared to those without ODT independent of the fluence used. However, as has already been mentioned in the previous paragraph, one has to be very cautious when simply deducing charge-carrier yields by comparing signal amplitudes, since the absolute cross sections of the charges are not exactly known, and as we have shown above, the spectrum of free charges appears to be different from the spectrum of trapped charges and CT states in samples prepared with ODT.

3. SUMMARY AND IMPLICATIONS FOR PHOTOVOLTAIC PERFORMANCE

Exciton Dissociation. The efficiency-limiting photophysical processes occurring in bulk heterojunction organic solar cells can be categorized into: (i) exciton relaxation of those excitons, which fail to undergo dissociation at a nearby heterojunction; (ii) geminate recombination of interfacial CT states; (iii) nongeminate recombination of separated/free charge carriers prior to the extraction from the device; and (iv) trap-assisted nongeminate recombination of those charges which are immobile in the blend. Typically the polymer exciton dissociation yield in polymer:fullerene blends is close to unity, since excitons are very efficiently quenched in well-intermixed blends. This loss channel can only be relevant if the domain size is comparable to the exciton diffusion length. In fact, diffusion-limited exciton quenching on a time scale of several picoseconds has previously been shown in annealed RR-P3HT:PCBM blends, where PCBM is expelled from the P3HT crystalline domains upon annealing, and thus polymer-rich domains of high crystallinity are formed.[52] However, even for the exceptional case of RR-P3HT with its well-ordered solid-state structure, the total loss due to diffusion-limited exciton dissociation does amount to a few percent only. Diffusion-limited polymer exciton quenching is also observed in the present study on PCPDTBT:PCBM blends for samples prepared with ODT as cosolvent, while instantaneous quenching of polymer excitons was found in samples prepared without ODT. The straightforward explanation is that ODT increases the demixing leading to larger PCPDTBT-rich domains. Excitons created within these polymer domains have to reach the heterojunction to undergo charge transfer, which in the present system occurred on a time scale of 10 ps. Our early time pump−probe experiments also exhibited a rise of the bleach and charge-induced absorption on a time scale of several tens of picoseconds for samples prepared without ODT and even hundreds of picoseconds for samples prepared with ODT. In fact, the intensity-independent rise of the bleach in conjunction with the charge-induced absorption can only be explained by delayed exciton dissociation of excitons originally created in PCBM-rich domains. We note that in our previous experiments on P3HT:PCBM and PCDTBT:PCBM samples, we could never observe such a rise of the charge-induced PA on a time scale similar to the rise observed for PCPDTBT:PCBM in this study, which would otherwise have pointed to a delayed charge generation due to excitons created in PCBM. The most likely explanation is that the aforementioned polymers exhibit much stronger absorption at the excitation wavelength of 532 nm, and thus excitons are mostly created in the polymer. The observation of a pronounced diffusion-limited PCBM exciton

dissociation in PCPDTBT:PCBM films independent of the use of solvent additives implies a wavelength dependence of the photophysical processes in these blends and requires further investigation, since it could be a potential loss process, if, for instance, excitons in PCBM recombine before reaching the interface or undergo intersystem crossing to triplet states due to the rather slow exciton diffusion process. Figure 10 schematically summarizes all processes together with their corresponding time scales for PCPDTBT:PCBM blend films prepared with and without the processing additive ODT.

The role of Interfacial CT States. The second loss channel that needs to be considered is relaxation of intermediate polaron pairs into strongly bound interfacial CT states followed by geminate recombination in competition with the formation of free charges from those "hot" electron−hole pairs that provide sufficient excess energy for the charges to overcome their mutual attraction. In fact, it is evident that a large fraction of the intermediate polaron pairs created by exciton dissociation collapses into strongly bound CT states, as we observe a pronounced signal decay of the bleach and the charge-induced absorption following a single exponential decay with an inverse rate of 700 ps (ODT) and 1200 ps (without ODT) (compare data in Figure 10). It is not straightforward to determine the total fraction of the CT state recombination from the pump−probe experiments, since the exact cross sections and spectra of the free charges and strongly bound CT states are unknown, and their individual absorption spectra are strongly superimposed. Nonetheless, our pump−probe experiments have demonstrated that the main process occurring in the first few nanoseconds is a fast and intensity-independent geminate recombination process. Hence, in the absence of competing processes, such as nongeminate recombination, the ground-state recovery can be used as an approximate measure of the fraction of excited states that return to the ground state after exciton dissociation. Using this approximation we have determined a total loss due to geminate recombination of about 50% in samples prepared without ODT and 30% in samples prepared with ODT. Our findings are in line with the earlier findings by the Blom group,[17] which showed a reduced fraction of geminate recombination in samples prepared with solvent additives determined by photocurrent measurements. The difference observed in our study is larger compared to the results reported earlier by Hwang et al.,[20] who showed only a weak impact of solvent additives on the fraction of geminate recombination. It is also worth mentioning that the excess thermal energy that an electron gains during charge transfer from PCPDTBT to PCBM is significantly less than for instance in P3HT:PCBM. This lesser excess energy may reduce the yield of free charges compared to P3HT:PCBM blends. The local morphology at the interface, for instance, the donor−acceptor distance certainly plays an additional and important role in the charge separation efficiency as recently reported by Holcombe et al.[53] One may further argue that the interactions between the molecules directly located at the interface (those which participate in the charge separation) and the molecules in the bulk of the polymer or fullerene (those which transport charges away from the interface) play an important role for efficient charge separation, as has recently been suggested for polymer:-perylenediimide blends.[54]

In fact, in highly crystalline materials, such as P3HT, an additional thermodynamic driving force exists that supports charge transport from the disordered interface to the more ordered bulk material. In lesser ordered materials, as in the present case of PCPDTBT:PCBM, this driving force is expected to be reduced if not entirely absent.

Recombination of Loosely Bound Polaron Pairs and Free Charges. Let us now discuss the long time (>1 ns) recombination dynamics of charges in PCPDTBT:PCBM blends. After about 3 ns we consider the pool of strongly bound interfacial CT states to be emptied in both samples, and it is expected that nongeminate recombination processes of free charge carriers govern the dynamics on a ns−μs time scale. However, in the sample prepared without ODT the ns−μs decay of the charge-induced absorption probed at the peak position appears to be a superposition of an intensity-independent process on a longer time scale up to 10 ns and an intensity-dependent recombination process. The latter can clearly be seen after several tens of nanoseconds, while the former occurs on a significantly longer time scale than the fast geminate recombination of strongly bound CT states that we observed in the early time pump−probe experiments. In addition, the weak intensity-dependence points to a geminate-like recombination process different from the subnanosecond recombination observed in the early time experiments. Geminate recombination on time scales even up to 100 ns has previously been reported and assigned to the recombination of loosely bound charge pairs that have not entirely escaped their mutual attraction.[55] One may also argue that these are charge pairs that are spatially trapped in isolated domains, where they cannot escape into the charge percolation network. The nanosecond recombination of loosely bound pairs is prominent in samples prepared without ODT, where it clearly occurs in addition to the subnanosecond geminate recombination of strongly bound interfacial CT states (sometimes referred to as CT-excitons) that we have identified in the early time pump−probe experiments. Thus, the geminate recombination of loosely bound charge pairs contributes to the loss processes in samples prepared without ODT, implying an unfavorable morphology for fast free charge formation.

It is an interesting question to be addressed in future work, whether these loosely bound polaron pairs, that recombine on the time scale of several nanoseconds, can undergo a field-assisted separation and thus could potentially contribute to the photocurrent in real devices. On the other hand, the occurrence of an intensity-dependent recombination at times longer than 10 ns indicates that a significant fraction of free charges has also been generated in samples prepared without ODT, which can indeed be extracted as photocurrent from the device. This is reasonable since devices prepared without ODT still exhibit a short circuit current of 4 mA/cm^2. Samples prepared with ODT demonstrate a very pronounced intensity dependence even on a time scale of several nanoseconds, implying that loosely bound polaron pairs are entirely absent and that nongeminate recombination dominates the dynamics at 1300 nm from the very beginning. By fitting the intensity-dependent dynamics to a Langevin recombination model, we obtained a nongeminate recombination coefficient of 1×10^{-8} $(\mathrm{cm}^3)^{\lambda}/\mathrm{s}$ and a recombination order of $\lambda + 1 = 1.86$. From the recombination coefficient and order, the effective (i.e., bimolecular) recombination coefficient for 3D Langevin-type recombination was calculated to 6.3×10^{-11} cm^3/s for a charge-carrier density of 5×10^{15} 1/cm^3. We have recently reported the recombination dynamics of charges in P3HT:PCBM and PCDTBT:PCBM probed by ns−ms transient absorption experiments and fitted the experimentally observed dynamics by a photophysical model, assuming that exciton dissociation leads to the

Table 2. Comparison of Effective Langevin Recombination Coefficients Calculated for a Charge Carrier Density of 5×10^{15} 1/cm^3

system	with ODT	without ODT	PCDTBT	rr-P3HT (as cast)	rr-P3HT (annealed)
γ_{eff}/cm^{3}s^{-1}	6.3×10^{-11}	3.2×10^{-11}	1.6×10^{-12}	1.5×10^{-12}	2.2×10^{-13}

population of two pools, i.e., interfacial CT states and free charge carriers, not interacting with each other.[6]

Table 2 summarizes the effective Langevin recombination coefficients obtained for the previously reported polymer:fullerene blends[6,51] and compares these values to those obtained for the PCPDTBT:PCBM blends presented in this study. One significant difference is apparent from the comparison with previous results. The recombination coefficient of the PCPDTBT:PCBM blends is more than 2 orders of magnitude larger compared to annealed RR-P3HT:PCBM and also more than 1 order of magnitude larger than obtained for PCDTBT:PCBM blends. Hence, it appears that nongeminate recombination of free charge carriers is significantly faster in PCPDTBT:PCBM blends. The recombination coefficients we obtained by pump−probe spectroscopy are also in excellent agreement with those recently reported by Albrecht et al., which in general further supports the validity of our measurements and data analysis.[21] The significantly larger nongeminate recombination coefficient observed for PCPDTBT:PCBM blends compared to, for instance, P3HT:PCBM implies that free charges more frequently encounter each other at the interface, and/or each encounter has a larger recombination probability in PCPDTBT:PCBM. A simple reason for the former could be a very high charge-carrier mobility in PCPDTBT:PCBM compared to P3HT:PCBM, which is, however, experimentally not observed as we will discuss later. Another reason for more frequent encounters of free charges in PCPDTBT:PCBM compared to P3HT:PCBM could be of thermodynamic origin. We have already discussed that in the exceptional case of P3HT:PCBM, the high crystallinity of the polymer creates an additional thermodynamic driving force that supports the separation of charges and their transport from the interface toward the bulk. Vice versa the same argument may explain the small nongeminate recombination coefficient observed for P3HT:PCBM in comparison to PCPDTBT:PCBM. While in the former holes are more likely to reside in the bulk of the polymer and transport toward the interface is expected to require energy, the generally higher disorder in the latter may reduce the energetic difference between interface and bulk, and thus charges can more easily approach the interface, where they can nongeminately recombine, before they can be extracted as photocurrent from the device.

In general nongeminate recombination of free charges competes with charge-carrier extraction, as we have previously shown for RR-P3HT:PCBM devices.[4] By measuring the bias dependence of nongeminate recombination for the latter, we have determined that at short circuit conditions, the fraction of nongeminate recombination is only about 2%, i.e., most of the carriers can be extracted in RR-P3HT:PCBM.[56] However, the fraction of nongeminate recombination significantly increases toward open circuit conditions, since the extraction rate of charges decreases due to the weaker internal electric field. Hence, a larger nongeminate recombination coefficient in PCPDTBT:PCBM implies that these devices suffer substantially from nongeminate losses, which certainly contributes to the low device fill factor. We note that the increased nongeminate recombination coefficient can be compensated by faster charge extraction due to a higher charge-carrier mobility. For that, mobility would have to be 2 orders of magnitude higher than observed for RR-P3HT:PCBM blends to compensate the fast nongeminate recombination in PCPDTBT:PCBM. This is experimentally not observed, for instance, Albrecht et al. reported that PCPDTBT:PCBM blends prepared with additives have a mobility similar to annealed RR-P3HT:PCBM samples.[21] When we probe the recombination dynamics in the longer wavelength NIR region, at around 1500 nm or beyond, we observe a much weaker intensity dependence of the recombination dynamics, indicating that the charges we monitor in this spectral region are different from those absorbing at the peak position of the charge-induced absorption, which is around 1300 nm in the blend prepared with ODT. Thus, it appears that here we observe mostly trapped charges undergoing a trap assisted rather than a Langevin-type recombination. The observation of a significant fraction of trapped charges is also in good agreement with previously reported transient photocurrent results by McNeill et al.[18]

Impact on Photovoltaic Performance. Let us finally comment on the implications of the recombination processes for the PCPDTBT:PCBM device performance. The total short circuit current that can be expected from a PCPDTBT:PCBM device, assuming that all absorbed photons generate free charges that thereafter can be extracted as photocurrent is 19 mA/cm^2. Our early time pump−probe experiments have shown that geminate recombination contributes to the charge-carrier loss at open circuit voltage and amounts to approximately 30%. Hence, geminate recombination alone would reduce J_{SC} to 11 mA/cm^2 at the measured light intensity around 0.86 suns, assuming that the magnitude is similar at short circuit conditions, which is a simplification, since free charge generation was recently shown to be field dependent in PCPDTBT:PCBM.[21] However, given that we observed a short circuit current of 7 mA/cm^2 at 0.86 suns in devices made with ODT as cosolvent, it is reasonable to assume that the reduction of the short circuit current is not only caused by geminate recombination but also by fast recombination of free charge carriers, as implied by the large nongeminate recombination coefficient. We have also observed that excitons do not only dissociate instantaneously but also by a diffusion-limited process, which is even more pronounced, when excitons are generated in PCBM domains. In addition we have observed some loosely bound polaron pairs in samples prepared without ODT, which recombine within several nanoseconds. Again, one may speculate that these loosely bound pairs can fully separate into free charges, if excess energy is provided by an electric field. The electric field dependence should then be more pronounced in samples prepared without ODT supported by recent time-delayed collection field experiments of the Neher group.[21] Further work will address the temperature and field dependence of the charge-induced absorption of free charges and CT states in the NIR probe range.

4. CONCLUSION

Exciton dissociation in PCPDTBT:PCBM blends led to the formation of free charges and strongly bound CT states, where the latter undergo geminate recombination with an inverse rate of 700 ps in samples prepared with ODT and 1200 ps in samples prepared without ODT. The fast subnanosecond geminate recombination caused a total loss of excited states of about 50% within the first 3 ns after photoexcitation in samples prepared without ODT, which severely limited the performance of PCPDTBT:PCBM solar cells. The fraction of subnanosecond geminate recombination was lowered to 30% in samples prepared with ODT as a solvent additive, implying a higher yield of free charge carriers. In addition to ultrafast exciton dissociation, diffusion-limited dissociation of excitons created within polymer-rich domains was observed on a time scale of 10 ps in samples prepared with ODT. The occurrence of diffusion-limited exciton dissociation was attributed to larger polymer-rich domains in samples prepared with ODT, where the increased domain size was proven by 2D $^{13}C\{^{1}H\}$ HETCOR solid-state NMR spectroscopy. Independent of the use of solvent additives diffusion-limited dissociation of excitons generated in PCBM-rich domains occurred in both blends, leading to an additional delayed formation of free charges and CT states on a time scale up to 50 ps in samples prepared without ODT and 300 ps in samples prepared with ODT. After the early time diffusion-limited exciton dissociation and subnanosecond geminate recombination of strongly bound CT states, the free charges in samples prepared with additives exclusively undergo nongeminate recombination with an effective recombination coefficient of 6.3×10^{-11} cm^3 s^{-1}, i.e., two orders of magnitude faster than previously observed for the P3HT:PCBM reference system, indicating that in PCPDTBT:PCBM nongeminate recombination efficiently competes with charge extraction. An additional nanosecond recombination component is observed in samples prepared without ODT and assigned to loosely bound polaron pairs that have not entirely managed to escape their mutual attraction. Triplet state formation appears to be of minor importance in PCPDTBT:PCBM blends as geminate recombination of CT states is too fast to allow efficient intersystem crossing.

■ ASSOCIATED CONTENT

Ⓢ Supporting Information

Experimental section, AFM images of blends, further TA spectra and dynamics, and EQE measurements on devices. This material is available free of charge via the Internet at http://pubs.acs.org.

■ AUTHOR INFORMATION

Corresponding Author

laquai@mpip-mainz.mpg.de

Notes

The authors declare no competing financial interest.

■ ACKNOWLEDGMENTS

F.L. is very grateful to the Max Planck Society for funding a Max Planck Research Group and acknowledges support within the priority program 1355 of the Deutsche Forschungsgemeinschaft (DFG). F.E. and M.M. thank the Max Planck Graduate Center for funding. I.A.H. acknowledges a fellowship of the Alexander von Humboldt Foundation. F.L. and F.E. thank D. Neher and E. Riedle for helpful discussions. N.F., S.J., and M.R.H. acknowledge the continuing support of Prof. Hans Wolfgang Spiess. We acknowledge financial support by the International Research Training Group 1404 and the SFB 625.

■ REFERENCES

(1) Krebs, F. C. *Sol. Energy Mater. Sol. Cells* **2009**, *93*, 394−412.
(2) Galagan, Y.; de Vries, I. G.; Langen, A. P.; Andriessen, R.; Verhees, W. J. H.; Veenstra, S. C.; Kroon, J. M. *Chem. Eng. Process.* **2011**, *50*, 454−461.
(3) Bakulin, A. A.; Rao, A.; Pavelyev, V. G.; van Loosdrecht, P. H. M.; Pshenichnikov, M. S.; Niedzialek, D.; Cornil, J.; Beljonne, D.; Friend, R. H. *Science* **2012**, *335*, 1340−1344.
(4) Mauer, R.; Howard, I. A.; Laquai, F. *J. Phys. Chem. Lett.* **2010**, *1*, 3500−3505.
(5) Guo, J.; Ohkita, H.; Benten, H.; Ito, S. *J. Am. Chem. Soc.* **2010**, *132*, 6154−6164.
(6) Howard, I. A.; Mauer, R.; Meister, M.; Laquai, F. *J. Am. Chem. Soc.* **2010**, *132*, 14866−14876.
(7) Peet, J.; Kim, J. Y.; Coates, N. E.; Ma, W. L.; Moses, D.; Heeger, A. J.; Bazan, G. C. *Nat. Mater.* **2007**, *6*, 497−500.
(8) Chu, T.-Y.; Lu, J.; Beaupré, S.; Zhang, Y.; Pouliot, J.-R. m.; Wakim, S.; Zhou, J.; Leclerc, M.; Li, Z.; Ding, J.; Tao, Y. *J. Am. Chem. Soc.* **2011**, *133*, 4250−4253.
(9) Zhou, H.; Yang, L.; Stuart, A. C.; Price, S. C.; Liu, S.; You, W. *Angew. Chem., Int. Ed.* **2011**, *50*, 2995−2998.
(10) Amb, C. M.; Chen, S.; Graham, K. R.; Subbiah, J.; Small, C. E.; So, F.; Reynolds, J. R. *J. Am. Chem. Soc.* **2011**, *133*, 10062−10065.
(11) Hou, J.; Chen, H.-Y.; Zhang, S.; Li, G.; Yang, Y. *J. Am. Chem. Soc.* **2008**, *130*, 16144−16145.
(12) Dennler, G.; Scharber, M. C.; Brabec, C. J. *Adv. Mater.* **2009**, *21*, 1323−1338.
(13) Mühlbacher, D.; Scharber, M.; Morana, M.; Zhu, Z.; Waller, D.; Gaudiana, R.; Brabec, C. *Adv. Mater.* **2006**, *18*, 2884−2889.
(14) Albrecht, S.; Schäfer, S.; Lange, I.; Yilmaz, S.; Dumsch, I.; Allard, S.; Scherf, U.; Hertwig, A.; Neher, D. *Org. Electron.* **2012**, *13*, 615−622.
(15) Agostinelli, T.; Ferenczi, T. A. M.; Pires, E.; Foster, S.; Maurano, A.; Müller, C.; Ballantyne, A.; Hampton, M.; Lilliu, S.; Campoy-Quiles, M.; Azimi, H.; Morana, M.; Bradley, D. D. C.; Durrant, J.; Macdonald, J. E.; Stingelin, N.; Nelson, J. *J. Polym. Sci., Part B: Polym. Phys.* **2011**, *49*, 717−724.
(16) Morana, M.; Azimi, H.; Dennler, G.; Egelhaaf, H.-J.; Scharber, M.; Forberich, K.; Hauch, J.; Gaudiana, R.; Waller, D.; Zhu, Z.; Hingerl, K.; van Bavel, S. S.; Loos, J.; Brabec, C. J. *Adv. Funct. Mater.* **2010**, *20*, 1180−1188.
(17) Lenes, M.; Morana, M.; Brabec, C. J.; Blom, P. W. M. *Adv. Funct. Mater.* **2009**, *19*, 1106−1111.
(18) Li, Z.; McNeill, C. R. *J. Appl. Phys.* **2011**, *109*, 074513−074520.
(19) Cho, S.; Lee, J. K.; Moon, J. S.; Yuen, J.; Lee, K.; Heeger, A. J. *Org. Electron.* **2008**, *9*, 1107−1111.
(20) Hwang, I. W.; Cho, S.; Kim, J. Y.; Lee, K.; Coates, N. E.; Moses, D.; Heeger, A. J. *J. Appl. Phys.* **2008**, *104*, 33706−33714.
(21) Albrecht, S.; Schindler, W.; Kurpiers, J.; Kniepert, J.; Blakesley, J. C.; Dumsch, I.; Allard, S.; Fostiropoulos, K.; Scherf, U.; Neher, D. *J. Phys. Chem. Lett.* **2012**, 640−645.
(22) Jamieson, F. C.; Agostinelli, T.; Azimi, H.; Nelson, J.; Durrant, J. R. *J. Phys. Chem. Lett.* **2010**, *1*, 3306−3310.
(23) Clarke, T.; Ballantyne, A.; Jamieson, F.; Brabec, C.; Nelson, J.; Durrant, J. *Chem. Commun.* **2009**, 89−91.
(24) Hwang, I. W.; Soci, C.; Moses, D.; Zhu, Z.; Waller, D.; Gaudiana, R.; Brabec, C. J.; Heeger, A. J. *Adv. Mater.* **2007**, *19*, 2307−2312.
(25) Grancini, G.; Martino, N.; Antognazza, M. R.; Celebrano, M.; Egelhaaf, H.-J.; Lanzani, G. *J. Phys. Chem. C.* **2012**, *116*, 9838−9844.
(26) Jarzab, D.; Cordella, F.; Gao, J.; Scharber, M.; Egelhaaf, H.-J.; Loi, M. A. *Adv. Energy Mater.* **2011**, *1*, 604−609.

(27) Scharber, M. C.; Lungenschmied, C.; Egelhaaf, H.-J.; Matt, G.; Bednorz, M.; Fromherz, T.; Gao, J.; Jarzab, D.; Loi, M. A. *Energy Environ. Sci.* **2011**, 5077−5083.
(28) Deschler, F.; Da Como, E.; Limmer, T.; Tautz, R.; Godde, T.; Bayer, M.; von Hauff, E.; Yilmaz, S.; Allard, S.; Scherf, U.; Feldmann, J. *Phys. Rev. Lett.* **2011**, *107*, 127402−127405.
(29) Di Nuzzo, D.; Aguirre, A.; Shahid, M.; Gevaerts, V. S.; Meskers, S. C. J.; Janssen, R. A. J. *Adv. Mater.* **2010**, *22*, 4321−4324.
(30) Tasios, N.; Grigoriadis, C.; Hansen, M. R.; Wonneberger, H.; Li, C.; Spiess, H. W.; Müllen, K.; Floudas, G. *J. Am. Chem. Soc.* **2010**, *132*, 7478−7487.
(31) Hansen, M. R.; Feng, X.; Macho, V.; Müllen, K.; Spiess, H. W.; Floudas, G. *Phys. Rev. Lett.* **2011**, *107*, 257801−257805.
(32) Saalwächter, K. *Prog. Nucl. Magn. Reson. Spectrosc.* **2007**, *51*, 1−35.
(33) Bohle, A.; Brunklaus, G.; Hansen, M. R.; Schleuss, T. W.; Kilbinger, A. F. M.; Seltmann, J.; Spiess, H. W. *Macromolecules* **2010**, *43*, 4978−4985.
(34) Rapp, A.; Schnell, I.; Sebastiani, D.; Brown, S. P.; Percec, V.; Spiess, H. W. *J. Am. Chem. Soc.* **2003**, *125*, 13284−13297.
(35) Khan, M.; Enkelmann, V.; Brunklaus, G. *J. Am. Chem. Soc.* **2010**, *132*, 5254−5263.
(36) Mafra, L.; Santos, S. M.; Siegel, R.; Alves, I.; Almeida Paz, F. A.; Dudenko, D.; Spiess, H. W. *J. Am. Chem. Soc.* **2011**, *134*, 71−74.
(37) Yang, C.; Hu, J. G.; Heeger, A. J. *J. Am. Chem. Soc.* **2006**, *128*, 12007−12013.
(38) Nieuwendaal, R. C.; Ro, H. W.; Germack, D. S.; Kline, R. J.; Toney, M. F.; Chan, C. K.; Agrawal, A.; Gundlach, D.; VanderHart, D. L.; Delongchamp, D. M. *Adv. Funct. Mater.* **2012**, *22*, 1255−1266.
(39) Chambon, S.; Mens, R.; Vandewal, K.; Clodic, E.; Scharber, M.; Lutsen, L.; Gelan, J.; Manca, J.; Vanderzande, D.; Adriaensens, P. *Sol. Energy Mater. Sol. Cells* **2012**, *96*, 210−217.
(40) Schmidt-Rohr, K.; Spiess, H. W. *Multidimensional Solid-State NMR and Polymers*; Academic Press Limited: London, U.K., 1994.
(41) van Rossum, B. J.; Förster, H.; de Groot, H. J. M. *J. Magn. Reson.* **1997**, *124*, 516−519.
(42) Bielecki, A.; Kolbert, A. C.; Levitt, M. H. *Chem. Phys. Lett.* **1989**, *155*, 341−346.
(43) Vanlaeke, P.; Swinnen, A.; Haeldermans, I.; Vanhoyland, G.; Aernouts, T.; Cheyns, D.; Deibel, C.; D'Haen, J.; Heremans, P.; Poortmans, J.; Manca, J. V. *Sol. Energy Mater. Sol. Cells* **2006**, *90*, 2150−2158.
(44) Rogers, J. T.; Schmidt, K.; Toney, M. F.; Kramer, E. J.; Bazan, G. C. *Adv. Mater.* **2011**, *23*, 2284−2288.
(45) Rogers, J. T.; Schmidt, K.; Toney, M. F.; Bazan, G. C.; Kramer, E. J. *J. Am. Chem. Soc.* **2012**, *134*, 2884−2887.
(46) Lu, H.; Akgun, B.; Russell, T. P. *Adv. Energy Mater* **2011**, *1*, 870−878.
(47) Lou, S. J.; Szarko, J. M.; Xu, T.; Yu, L.; Marks, T. J.; Chen, L. X. *J. Am. Chem. Soc.* **2011**, *133*, 20661−20663.
(48) Dimitrov, S. D.; Nielsen, C. B.; Shoaee, S.; Shakya Tuladhar, P.; Du, J.; McCulloch, I.; Durrant, J. R. *J. Phys. Chem. Lett.* **2011**, *3*, 140−144.
(49) Albert-Seifried, S.; Friend, R. H. *Appl. Phys. Lett.* **2011**, *98*, 223304−223303.
(50) Zhang, F.; Jespersen, K. G.; Björström, C.; Svensson, M.; Andersson, M. R.; Sundström, V.; Magnusson, K.; Moons, E.; Yartsev, A.; Inganäs, O. *Adv. Funct. Mater.* **2006**, *16*, 667−674.
(51) Etzold, F.; Howard, I. A.; Mauer, R.; Meister, M.; Kim, T.-D.; Lee, K.-S.; Baek, N. S.; Laquai, F. *J. Am. Chem. Soc.* **2011**, *133*, 9469−9479.
(52) Agostinelli, T.; Lilliu, S.; Labram, J. G.; Campoy-Quiles, M.; Hampton, M.; Pires, E.; Rawle, J.; Bikondoa, O.; Bradley, D. D. C.; Anthopoulos, T. D.; Nelson, J.; Macdonald, J. E. *Adv. Funct. Mater.* **2011**, *21*, 1701−1708.
(53) Holcombe, T. W.; Norton, J. E.; Rivnay, J.; Woo, C. H.; Goris, L.; Piliego, C.; Griffini, G.; Sellinger, A.; Brédas, J.-L.; Salleo, A.; Fréchet, J. M. J. *J. Am. Chem. Soc.* **2011**, *133*, 12106−12114.
(54) Pensack, R. D.; Guo, C.; Vakhshouri, K.; Gomez, E. D.; Asbury, J. B. *J. Phys. Chem. C* **2012**, *116*, 4824−4831.
(55) Pal, S. K.; Kesti, T.; Maiti, M.; Zhang, F.; Inganäs, O.; Hellström, S.; Andersson, M. R.; Oswald, F.; Langa, F.; Österman, T.; Pascher, T.; Yartsev, A.; Sundström, V. *J. Am. Chem. Soc.* **2010**, *132*, 12440−12451.
(56) Mauer, R.; Howard, I. A.; Laquai, F. *J. Phys. Chem. Lett.* **2011**, *2*, 1736−1741.